INVERSION ALGORITHM FOR ESTIMATING RADIO FREQUENCY INTERFERENCE CHARACTERISTICS BASED ON KURTOSIS MEASUREMENTS

Sidharth Misra and Christopher Ruf, *Fellow, IEEE*

Department of Atmospheric, Oceanic and Space Sciences
University of Michigan
Ann Arbor, MI 48109-2143

Abstract - An inversion algorithm is developed to recover power and duty-cycle of incoming Radio Frequency Interference (RFI) signals from kurtosis. The algorithm applies simulated annealing on multiple kurtosis values obtained from different radiometer integration periods. The paper evaluates the performance of the inversion algorithm by performing Monte-Carlo simulations to obtain error statistics. The inversion capability of the algorithm and its robustness against the 50% duty-cycle blind-spot (generally present for the kurtosis detection algorithm) is demonstrated using experimental data.

***Index terms* – Microwave radiometry, radio frequency interference, Simulated Annealing**

I. INTRODUCTION

Microwave remote-sensing measurements made in the L, C and even X-band are susceptible to man-made Radio Frequency Interference signals [2,4,5,7,8]. Many analog and digital techniques have been developed that use spectral or temporal gridding to detect RFI [3,6,9,11]. The kurtosis detection algorithm uses statistical techniques to identify RFI corrupted data [10]. The algorithm checks the normality of the incoming natural thermal emission by measuring higher order central moments of the pre-detection voltage and calculates the kurtosis by taking the ratio of the 4^{th} central moment to the square of the 2^{nd} central moment. If the ratio deviates from 3, then the data contains non-Gaussian (likely man-made) interference and is tagged as being RFI-corrupted.

RFI at L-Band often originates from radars [12] and is modeled as a pulsed-sinusoidal signal. The detectability of the kurtosis algorithm is dependent on the duty-cycle and strength of the RFI [1]. The kurtosis detection algorithm performs better with higher strength RFI and with low duty-cycle signals. The accumulation period over which the central moments are calculated influences both the time-average strength and the effective duty-cycle of the RFI and, thus, the performance of the kurtosis detection algorithm. If the duty-cycle and strength of the RFI are known, an optimum accumulation period can be found to improve detectability. Also, the kurtosis detection algorithm is blind to RFI with a 50% duty-cycle. This handicap can be avoided by varying the sample integration time if the duty-cycle is known. Finally, knowledge of the strength of the RFI can help improve the mitigation process by eliminating only problematic RFI. For example, since soil moisture measurements require a sensitivity of approximately 1K, mitigating a 0.1K RFI biased sample is unnecessary. In addition to the above advantages, obtaining RFI parameters is a useful technique for system identification purposes.

An estimation algorithm has been developed to determine the strength and duty cycle of RFI directly from raw ADD samples. The estimator requires measurements of the central moments, and hence of the kurtosis, at multiple integration times. A forward model has been developed which predicts the kurtosis for each integration time for a given combination of RFI signal strength and duty-cycle. The forward model is inverted by the estimator. Due to the highly non-linear nature of the forward model, three separate inversion techniques were tested. The simulated annealing algorithm was finally implemented. Initial theoretical and empirical results indicate that the algorithm can successfully invert duty-cycle and power from kurtosis values. The algorithm is also implemented on field data obtained during a flight campaign over the continental U.S.

The next section discusses the theory behind the kurtosis detection algorithm as well as the inversion algorithm. The error statistics of a simulated annealing inversion are shown in Section III. Section IV presents experimental results of the inversion algorithm identifying blind spot duty cycle signals, as well as successfully recovering RFI parameters. Finally, the last section summarizes and discusses the results.

II. DETECTION/INVERSION ALGORITHM AND RFI MODEL

The RFI detection algorithm works on the principle of measuring the deviation from normality of the incoming thermal emission. Incoming thermal emissions are random in nature and follow a Gaussian distribution, whereas RFI is man-made and non-normal. The detection algorithm measures the higher order central moments of the incoming signal and measures the kurtosis ratio as shown by (1). If

the ratio is 3 (within some standard deviation) then the signal is RFI free.

$$k = \frac{\left\langle \left(x(t) - \langle x(t) \rangle\right)^4 \right\rangle}{\left\langle \left(x(t) - \langle x(t) \rangle\right)^2 \right\rangle^2} \quad (1)$$

where, < > represents the expectation operator and x represents the incoming thermal signal. The RFI signal itself is modeled as a simplified radar-like pulsed sinusoidal signal [15] with a characteristic duty-cycle (d) and power (S) as shown by (2).

$$x[n] = \begin{cases} a[n] & m \le n \le M \\ a[n] + A\sin(2\pi f_o n) & else \end{cases} \quad (2)$$

where $a \sim N(\mu,\sigma)$ is a normally distributed signal, A is the amplitude of the pulsed-sinusoid signal, f_o represents frequency of the RFI uniformly distributed between 0 and 0.5 (0 is DC and 0.5 is the Nyquist rate), M represents the total integration period in units of samples. The duty cycle of the sinusoidal pulse is therefore given by $d=m/M$ and relative power is given by $S=dA^2/2\sigma^2$.

The inversion algorithm is based on the principle of obtaining multiple kurtosis ratio values for different sub-sampling periods within the total sampling period. The following forward model (3) obtained from [1] is used within the inversion algorithm for generating kurtosis values for different values of power S and duty-cycle d. Different sub-sampling periods (N) impact S and d and hence affect the kurtosis ratio k. Thus we have two unknowns (S,d) that can be estimated from multiple measurements of k obtained from different sub-sampling periods N.

$$\bar{k}(S,d) = 3\frac{\left(1 + 2S + \frac{1}{2d}S^2\right)}{(1+S)^2} \quad (3)$$

Due to the non-linearity of the forward model, in order to avoid local minima issues, simulated annealing [13,14] is used for inverting the RFI parameters. Simulated annealing starts by selecting an initial high annealing temperature and a random solution (S_o,d_o) to be inverted from some kurtosis vector k. An initial energy state is calculated by comparing the original k and the estimated k obtained by sending the solution through the forward model. The lower the energy state, the better the solution. Random solutions are then selected and their energy states are calculated. If the energy state is lower then the solution might be accepted, and if it is higher then it might be accepted based on some particular probability that is a function of the annealing temperature. The probability of a worse solution being accepted is higher for high annealing temperatures. This allows the solution not to be limited to the local minima. After a set number of iterations, a particular solution is accepted, the annealing temperature is lowered and the process is repeated again. The assumption made while inverting the RFI parameters are that the total integration period contains a single RFI pulse. In case of multiple pulses, a residual error analysis can be performed and the total integration period can be reduced i.e. the number of obtained kurtosis measurements (equations) can be reduced such that only one pulse is within the total integration period.

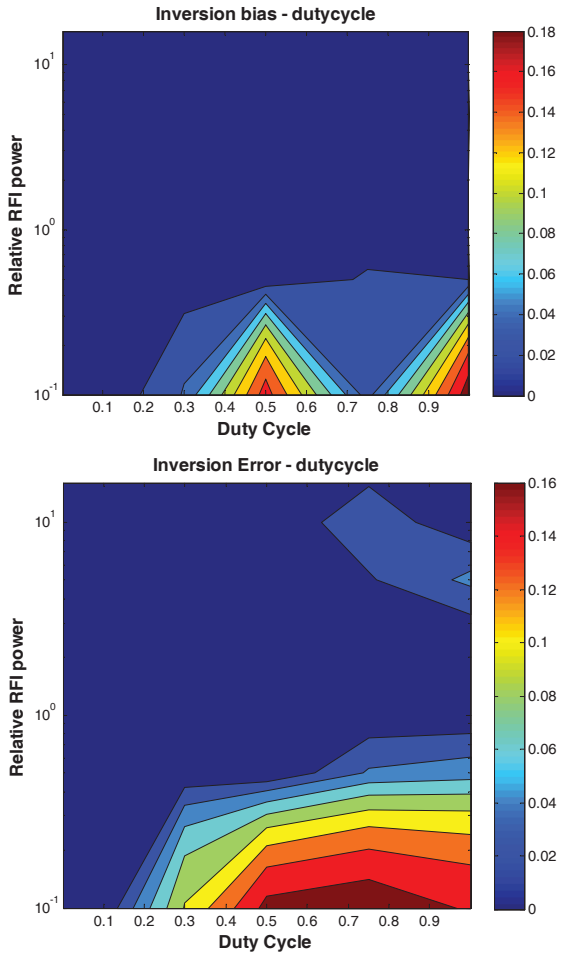

Fig.1. Bias (top plot) and standard deviation (bottom plot) of recovered duty cycle after performing simulated annealing inversion.

III. ERROR STATISTICS

Assuming the RFI model presented above Monte-Carlo simulations were performed to estimate the bias, error (standard deviation) and covariance of the inverted duty-cycle and power measurements obtained from the kurtosis ratio vector. Figures 1 and 2 show the bias and error of the inverted duty-cycle and power respectively. Kurtosis values are relatively larger for low duty-cycle as well as high power RFI. As expected, from Fig. 1, the inverted duty-

cycle has a certain amount of bias and error for RFI signals with relatively high duty-cycle and low power. The inverted power measurements on the other hand seem to have a relatively larger bias and error for high power, high duty-cycle RFI signals. This might be due to the fact that the solution space used by simulated annealing inversion is discrete and the resolution is not fine enough around higher power levels. This issue can possibly be solved by combining simulated-annealing inversion with other traditional inversion techniques such as the Newton-Raphson.

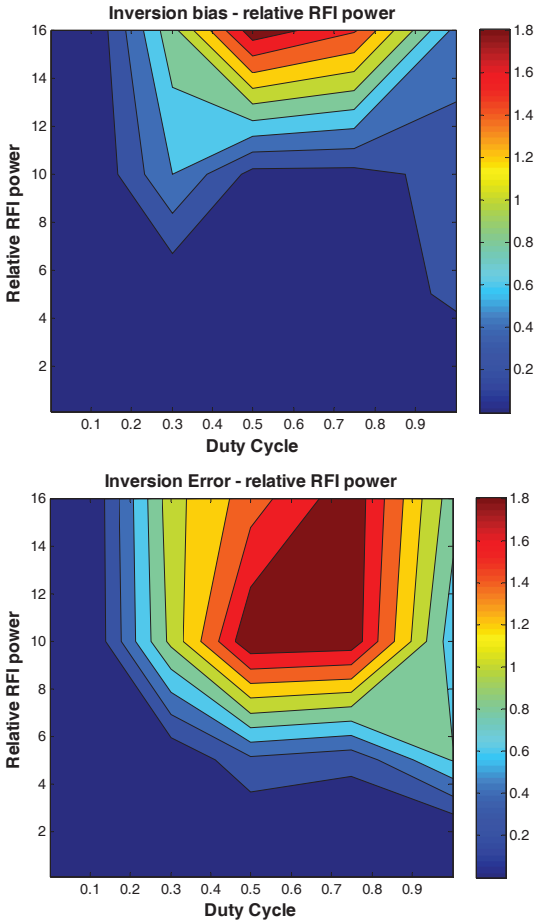

Fig.2. Bias (top plot) and standard deviation (bottom plot) of recovered relative RFI power after performing simulated annealing inversion.

Inversion covariance statistics are shown by Fig. 3. As expected, there is some amount of correlation between power and duty-cycle after inversion. The relationship between power and duty-cycle is noted in Section II.

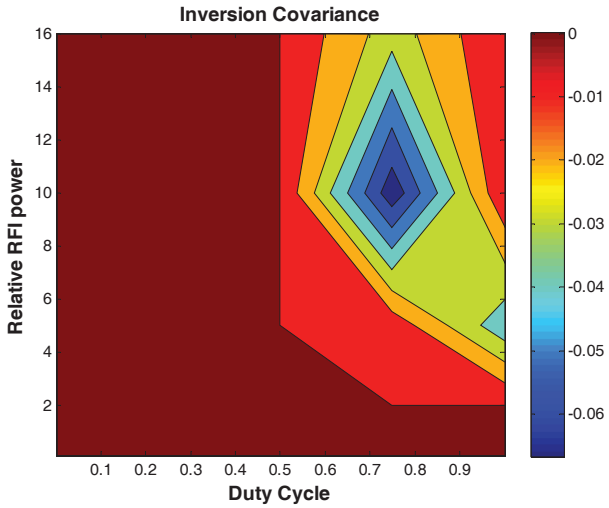

Fig.3. Covariance between recovered duty-cycle and relative RFI power after performing simulated annealing inversion.

IV. INVERSION RESULTS

The kurtosis detection algorithm has a blind-spot if the duty-cycle of RFI is 50% relative to the integration period. Fig. 4 below shows clear RFI spikes observed in the second moment (top plot) not picked up by kurtosis (middle plot). If the inversion algorithm is implemented, these sub-sampled integration times are combined together and the blind-spot problem is eliminated as seen in the bottom plot of the figure around 0 and 0.3 seconds. The middle plot in Fig. 4 has a spike around 0.6 sec because the pulse is spread across two separate integration periods, effectively reducing the duty-cycle below 50%.

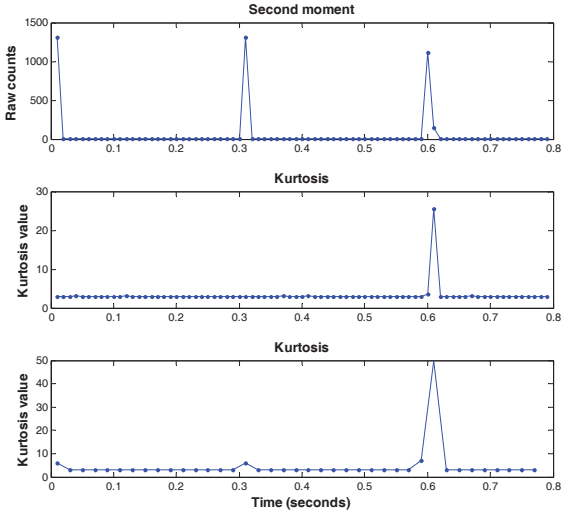

Fig. 4. Plot indicating the blind-spot of the kurtosis algorithm – Top plot: Raw second moment counts (power) indicating spikes with a 50% relative duty-cycle pulse-width, Middle plot: Kurtosis calculated at unit integration time, Bottom plot: Kurtosis calculated at twice the integration time of top two plots.

Fig. 5 is a scatter plot indicating duty-cycle recovered from empirical data vs. actual duty-cycle fed into the radiometer-kurtosis detector system. The power level of the incoming RFI was reduced over several steps for the same duty-cycle. As noted in the figure, the inversion algorithm performs very well in recovering the incoming duty-cycle of the signal, with a few outlier scatter points occurring due to relatively low input RFI power level. It should be noted that the performance of the inversion algorithm can be further improved and the width of the scatter reduced if the discrete solution space is further resolved.

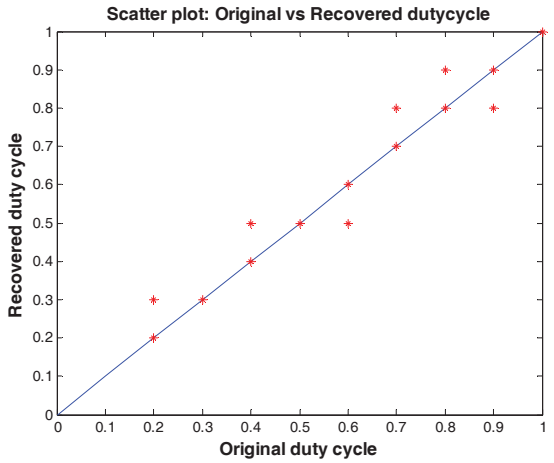

Fig. 5 Scatter plot indicating performance of the inversion algorithm by comparing recovered duty-cycle values with respect to original duty-cycle

V. CONCLUSION

The value of the kurtosis ratio depends not only on the characteristics of the incoming RFI, such as duty-cycle and power, but also on the number of samples used within an integration period. This property is used to obtain multiple kurtosis values and recover RFI characteristics using the simulated annealing inversion technique. Monte-Carlo simulations indicate that the inversion algorithm performs very well while recovering duty-cycle values. Kurtosis values are low for low power levels and high duty-cycle. The recovered duty-cycle values have relatively more error and bias associated with them around these regions. The recovered relative RFI power on the other hand indicates a higher bias and standard deviation for high power RFI signals. This might be due to the fact that the solution space is sparse around the high power levels. The performance of the algorithm can be improved by increasing the solution resolution.

Applying the inversion algorithm on empirical data indicates the ability of the inversion algorithm to detect 50% duty-cycle signals even though the kurtosis detection algorithm has a blind-spot for those types of signals. Scatter plots also indicate the ability of the simulated annealing algorithm to successfully recover duty-cycle values from empirical data. The algorithm can be further improved by combining it with a Newton-Raphson inversion method and by removing a few assumptions, such as a single pulse within a total integration period.

REFERENCES

[1] De Roo, R., S. Misra and C. Ruf (2007). "Sensitivity of the Kurtosis Statistic as a Detector of Pulsed Sinusoidal RFI," *IEEE Trans. Geosci. Remote Sens.*, 45(7), 1938-1946.

[2] Ellingson, S.W. and J.T. Johnson (2006). "A polarimetric survey of radio frequency interference in C- and X-bands in the continental United States using WindSat radiometry," *IEEE Trans. Geosc. Remote Sens.*, 44, 540-548.

[3] Guner, B., J.T. Johnson and N. Niamsuwan (2007). "Time and frequency blanking for radio frequency interference mitigation in microwave radiometry," *IEEE Trans. Geosci. Remote Sens.*, 45, 3672-3679.

[4] Li, L., et al. (2004). "A preliminary survey of radio-frequency interference over the U.S. in Aqua AMSR-E data," *IEEE Trans. Geosci. Remote Sens.*, 42(2), 380-380.

[5] Li, L., P.W. Gaiser, and M. Bettenhausen (2006). "WindSat radio-frequency interference signature and its identification over land and ocean," *IEEE Trans. Geosci. Remote Sens.*, 44(3), 530-539.

[6] Niamsuwan, N., J.T. Johnson and S.W. Ellingson (2005). "Examination of a simple pulse blanking technique for RFI mitigation," *Radio Science*, 40.

[7] Njoku E.G., P. Ashcroft, T.K. Chan, L. Li (2005). "Global survey and statistics of radio-frequency interference in AMSR-E land observations" *IEEE Trans. Geosci. Remote Sens.*, 43(5), 938–947.

[8] Njoku E., T. Chan, W. Crosson and A. Limaye (2004). "Evaluation of the AMSR-E Data Calibration over Land", *Rivista Italiana di Telerilevamento - Italian J. Remote Sens.*, 30/31, 15-33.

[9] Piepmeier, J.R., P. Mohammed and J. Knuble (2008). "A double detector for RFI mitigation in microwave radiometers," *IEEE Trans. Geosci. Remote Sens.*, 46, 458-465

[10] Ruf, C.S., S. M. Gross and S. Misra (2006). "RFI Detection and Mitigation for Microwave Radiometry with an Agile Digital Detector," *IEEE Trans. Geosci. Remote Sens.*, 44(3), 694-706.

[11] S. Misra and Ruf, C.S., (2008) "Detection of Radio Frequency Interference for the Aquarius radiometer," *IEEE Trans. Geosci. Remote Sens.*, 46(10), 3123-3128

[12] J.R. Piepmeier and F.A. Pellerano, "Mitigation of terrestrial radar interference in L-band spaceborne microwave radiometers," *Proc. IGARSS*, Denver, CO, 2006, pp. 2292-2296.

[13] Kirkpatrick, S., Gelatt Jr., C.D., and Vecchi, M.P., "Optimization by Simulated Annealing," *Science,* vol. 220, no. 4598, May 1983.

[14] Ruf, C.S., "Numerical annealing of low-redundancy linear arrays," *IEEE Trans. Antennas and Propagation.,* 41(1), Jan. 1993, 85-90.

[15] Johnson, J.T., and Potter, L.C., "Performance study of algorithms for detecting pulsed sinusoidal interference in microwave radiometry," *IEEE Trans. Geosci. Remote Sens.,* 47(2), 628-636